

Lossless Convexification of Powered-Descent Guidance with Non-Convex Thrust Bound and Pointing Constraints

John M. Carson III, Behçet Açıkmüşe, and Lars Blackmore

Abstract—A numerically-efficient, convex formulation of PDG (Powered-Descent Guidance) for Mars pinpoint and precision landing has been enhanced to include thrust pointing constraints. The original algorithm was designed to enforce both control and state constraints, including maximum and minimum thrust bounds, maximum speed limits and descent within a glideslope cone (surface impact avoidance). The thrust bounds are non-convex, so the original formulation developed a lossless convexification of these constraints. Likewise, thrust pointing constraints are non-convex. In this paper we present a relaxation for the thrust pointing constraint such that the enhanced PDG algorithm generates a lossless convexification for both the thrust bound and thrust pointing constraints. Pointing constraints are needed for onboard terrain-relative sensors that have specific field-of-view requirements during landing.

I. INTRODUCTION

A typical Mars EDL (Entry, Descent and Landing) consists of a hypersonic entry phase, a parachute phase and a landing phase. The landing phase typically implements either an air-bag system or a powered-descent system (throttleable rockets that descend the lander). Landing errors relative to an intended target are accumulated primarily between the atmospheric entry through parachute phases, with the daily variations in the Mars atmosphere being the dominant cause. The current state of practice in EDL has a landing capability of 10 km (3σ) from the desired landing target [1].

Landing systems using powered-descent thrusters offer the potential for greatly reducing the 10-km landing error and enabling precision and pinpoint landing. Powered-descent thrust profiles are generated with onboard guidance algorithms. Current guidance methods ensure a safe landing that avoids impact with the descending parachute/backshell after lander separation, but there is no attempt to minimize landing error. To reduce landing error, many candidate guidance algorithms have been developed [1]–[9]. These algorithms vector available thrust to maneuver the descending lander closer to the original target, thus achieving touchdown closer to a desired science location (or existing surface asset) and reducing the risk of any lengthy rover traverse.

Powered-descent guidance algorithms that minimize landing error must consider spacecraft performance constraints such as the governing physics, available fuel, thrust limits, and position and speed constraints. Additionally, the short duration of Mars powered descent requires computationally-efficient algorithms. The descent thrusters typically cannot

be throttled off after ignition, so guidance algorithms must constraint thrust profiles within a minimum and maximum bound. Further, onboard sensors for terrain-relative navigation generally require specific viewing orientations that constraint spacecraft attitude, and thus, thrust-pointing direction.

Many heritage PDG algorithms solve a close-form, simplified guidance problem by assuming polynomial profiles and ignoring some constraints [5], [10]. These approaches provide guidance solutions that have a limited envelop of initial states from which a spacecraft can maneuver toward the desired target without violating the physical state and control constraints [11]. Other methods enforce the appropriate constraints but with nonlinear optimization [6], [7], which has no guarantee on convergence time or that the most fuel optimal solution will be found.

The development of a convex PDG algorithm for pinpoint landing explicitly enforces state and control constraints and provides guarantees of global optimality and numerical efficiency [1]. A primary theoretical contribution from this work was the lossless convexification of the thrust-magnitude lower bound. Extensions of the algorithm for precision landing [2] considered landing situations where fuel availability limited the ability to remove all landing error. This paper revisits this convex formulation and incorporates an extension and theoretical proof that enforce thrust-pointing constraints. This is a significant theoretical contribution, as the non-convex thrust-pointing constraints, like the thrust-magnitude bounds, are convexified through a further lossless relaxation. The algorithm and proof also incorporate planetary rotation.

The enhanced convex PDG algorithm is formulated as a SoCP (Second order Cone Program) that can be solved with numerically-efficient interior-point solvers that have deterministic stopping criteria [12]. If a feasible solution exists, then interior-point methods will find the global optimal solution to an SoCP [13]. The explicit enforcement of the lower bound on thrust magnitude and the numerical efficiency and accuracy make the convex PDG algorithm a strong candidate for flight implementation [9]. Additionally, compared to heritage algorithms, the convex PDG algorithm provides a significant increase in the initial states from which pinpoint landing can be achieved [11].

II. PLANETARY SOFT LANDING PROBLEM WITH POINTING CONSTRAINTS

The planetary pinpoint landing problem searches for the thrust profile T_c and accompanying translational state trajectory $(\mathbf{r}, \dot{\mathbf{r}})$ that minimize fuel consumption and guide a lander from the initial position \mathbf{r}_0 and velocity $\dot{\mathbf{r}}_0$ to a

Authors are with the Jet Propulsion Laboratory, California Institute of Technology, 4800 Oak Grove Dr., M/S 198-326, Pasadena, CA 91109, USA. Email: {jmcarson, behcet, lars}@jpl.nasa.gov

©2010 California Institute of Technology. Government sponsorship acknowledged.

state of rest at the desired surface location. The problem considers planets with a constant rotation rate, a uniform gravity field, and negligible aerodynamic forces during the powered-descent phase of landing. When the target point is unreachable from a given initial state, a precision landing problem (or *minimum landing error* problem) is considered instead, with the objective to first find the closest reachable surface location to the target and second to obtain the minimum fuel state trajectory to that closest point. We formulate a prioritized optimization approach that handles both problems under a unified framework, which is then referred to as the *planetary soft landing problem*.

The dynamics of the system are described by

$$\begin{aligned}\dot{\mathbf{x}}(t) &= A(\boldsymbol{\omega}) \mathbf{x}(t) + B \left(\mathbf{g} + \frac{\mathbf{T}_c(t)}{m(t)} \right), \\ \dot{m}(t) &= -\alpha \|\mathbf{T}_c(t)\|,\end{aligned}\quad (1)$$

where $\mathbf{x}(t) = (\mathbf{r}(t), \dot{\mathbf{r}}(t)) : \mathbb{R}_+ \rightarrow \mathbb{R}^6$, $m(t) : \mathbb{R}_+ \rightarrow \mathbb{R}_+$ is lander mass, $\mathbf{g} \in \mathbb{R}^3$ is constant gravity,

$$A(\boldsymbol{\omega}) = \begin{bmatrix} \mathbf{0} & \mathbf{I} \\ -S(\boldsymbol{\omega})^2 & -2S(\boldsymbol{\omega}) \end{bmatrix}, \quad B = \begin{bmatrix} \mathbf{0} \\ \mathbf{I} \end{bmatrix}, \quad (2)$$

$\alpha > 0$ is constant fuel consumption (mass depletion) rate, $\boldsymbol{\omega} = (\omega_1, \omega_2, \omega_3)^T \in \mathbb{R}^3$ is constant planetary angular velocity, and $S(\boldsymbol{\omega})$ is a matrix representation of cross product $\boldsymbol{\omega} \times (\cdot)$.

The state constraints include a glide slope constraint and a maximum speed constraint. The glide slope constraint ensures that the lander position is a safe distance from the surface until the target is reached (Figure 1). The speed constraint is needed to avoid supersonic velocities (for planets with atmospheres) where the control thrusters can become unreliable. Both of these constraints are convex, and a convex set \mathbf{X} of feasible positions and velocities is defined as

$$\begin{aligned}\mathbf{X} &= \{(\mathbf{r}, \dot{\mathbf{r}}) \in \mathbb{R}^6 : \|\dot{\mathbf{r}}\| \leq V_{\max}, \\ &\quad \|E(\mathbf{r} - \mathbf{r}(t_f))\| - \mathbf{c}^T(\mathbf{r} - \mathbf{r}(t_f)) \leq 0\},\end{aligned}\quad (3)$$

where V_{\max} is the maximum allowable speed, and \mathbf{c} specifies the glideslope cone with angle γ_{gs} and vertex $\mathbf{r}(t_f)$:

$$\mathbf{c} \triangleq \frac{\mathbf{e}_1}{\tan \gamma_{\text{gs}}}, \quad \gamma_{\text{gs}} \in (0, \pi/2). \quad (4)$$

For completeness, we give the standard definition of the interior of \mathbf{X} :

$$\text{int}\mathbf{X} \triangleq \{\mathbf{x} \in \mathbf{X} : \exists \varepsilon > 0 \text{ such that } \mathbf{y} \in \mathbf{X} \text{ if } \|\mathbf{x} - \mathbf{y}\| < \varepsilon\}. \quad (5)$$

The boundary of \mathbf{X} is given by $\partial\mathbf{X} \triangleq \{x \in \mathbf{X} : x \notin \text{int}\mathbf{X}\}$.

Three control constraints are imposed in powered-descent guidance (Figure 2). Given the maneuver time (time-of-flight) t_f , for all $t \in [0, t_f]$, the control constraints include the following:

- Convex upper bound on thrust, $\|\mathbf{T}_c(t)\| \leq \rho_2$.
- Non-convex lower bound on thrust, $\|\mathbf{T}_c(t)\| \geq \rho_1 > 0$.
- Thrust pointing constraint $\hat{\mathbf{n}}^T \mathbf{T}_c(t) / \|\mathbf{T}_c(t)\| \geq \cos \theta$ where $\|\hat{\mathbf{n}}\| = 1$ is a direction vector and $0 \leq \theta \leq \pi$ is the maximum allowable angle from $\hat{\mathbf{n}}$; convex when $\theta \leq \pi/2$ and non-convex when $\theta > \pi/2$.

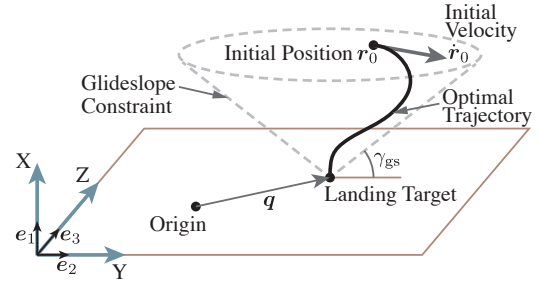


Fig. 1. Glideslope constraint in precision-landing PDG problem. The glideslope constraint requires the spacecraft to remain in a cone defined by the minimum slope angle γ_{gs} .

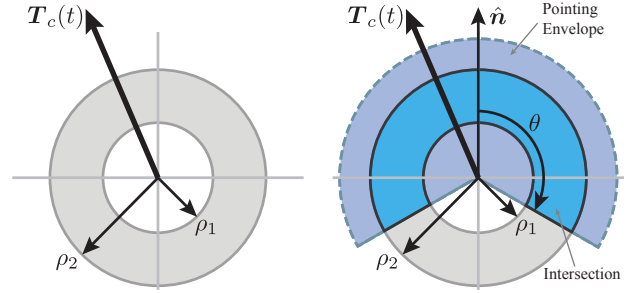


Fig. 2. Planar representation of original thrust bounds (left) and intersection of thrust bounds and thrust pointing limits (right)

Given the constraints, the dynamics, and a target location on the surface $(0, \mathbf{q})^T$ where $\mathbf{q} \in \mathbb{R}^2$ are the surface landing coordinates, the planetary soft landing problem is formulated as the following prioritized optimization problem:

Problem 1: Non-convex minimum landing error problem

$$\min_{t_f, \mathbf{T}_c} \|E\mathbf{r}(t_f) - \mathbf{q}\| \quad (6)$$

subject to the following, $\forall t \in [0, t_f]$: the dynamics in (1),

$$0 < \rho_1 \leq \|\mathbf{T}_c(t)\| \leq \rho_2, \quad \hat{\mathbf{n}}^T \mathbf{T}_c(t) \geq \|\mathbf{T}_c(t)\| \cos \theta, \quad (7)$$

$$m(0) = m_0, \quad m(t_f) \geq m_0 - m_f > 0, \quad (8)$$

$$\mathbf{x}(t) \in \mathbf{X}, \quad (9)$$

$$\mathbf{r}(0) = \mathbf{r}_0, \quad \dot{\mathbf{r}}(0) = \dot{\mathbf{r}}_0, \quad \mathbf{e}_1^T \mathbf{r}(t_f) = 0, \quad \dot{\mathbf{r}}(t_f) = \mathbf{0} \quad (10)$$

Problem 2: Non-convex minimum fuel problem

$$\max_{t_f, \mathbf{T}_c} m(t_f) - m(0) = \min_{t_f, \mathbf{T}_c(\cdot)} \int_0^{t_f} \alpha \|\mathbf{T}_c(t)\| dt \quad (11)$$

subject to the following, $\forall t \in [0, t_f]$: the dynamics in (1),

$$0 < \rho_1 \leq \|\mathbf{T}_c(t)\| \leq \rho_2, \quad \hat{\mathbf{n}}^T \mathbf{T}_c(t) \geq \|\mathbf{T}_c(t)\| \cos \theta,$$

$$\mathbf{x}(t) \in \mathbf{X}, \quad m(0) = m_0, \quad m(t_f) \geq m_0 - m_f > 0,$$

$$\mathbf{r}(0) = \mathbf{r}_0, \quad \dot{\mathbf{r}}(0) = \dot{\mathbf{r}}_0, \quad \mathbf{e}_1^T \mathbf{r}(t_f) = 0, \quad \dot{\mathbf{r}}(t_f) = \mathbf{0},$$

$$\|E\mathbf{r}(t_f) - \mathbf{q}\| \leq \|\mathbf{d}_{\text{P1}}^* - \mathbf{q}\| \quad (12)$$

where $\mathbf{d}_{\text{P1}}^* = E\mathbf{r}_{\text{P1}}^*(t_f) \in \mathbb{R}^2$ is obtained by solving Problem 1; \mathbf{d}_{P1}^* is the closest reachable point on the surface to the target location \mathbf{q} . Parameter m_f is the available fuel, m_0 is the wet mass at powered-descent ignition, and

$$E = \begin{bmatrix} \mathbf{e}_2^T \\ \mathbf{e}_3^T \end{bmatrix} = \begin{bmatrix} 0 & 1 & 0 \\ 0 & 0 & 1 \end{bmatrix}.$$

Equation (8) defines the initial lander mass and ensures that no more fuel than available is used. Equation (10) defines the initial and final position and velocity of the lander; the final state at time t_f constrains the lander to be at rest at the landing target. Note, the time-of-flight t_f is an optimization variable and not fixed *a priori*.

A key challenge in solving Problems 1 and 2 are the non-convex control constraints. The lower thrust-magnitude bound ρ_1 in (7) makes the allowable thrust a non-convex set (See Figure 2, left). When $\rho_1 = 0$ the thrust bound constraint is convex, but the thrust pointing constraint in (7) can still be non-convex when $\theta > \pi/2$ (See Figure 2, right). These non-convex control constraints prevent direct use of convex optimization techniques to solve this problem. Further, the $\dot{m}(t)$ mass-consumption dynamics in (1) are a nonlinear differential equation, which when discretized become nonlinear equality constraints (also non-convex).

The key theoretical innovations in Ref. [1] were a lossless convexification of Problem 2 (without thrust pointing constraints) that included a relaxation for the non-convex thrust bound and a method to handle the mass consumption dynamics. The optimal solution of the relaxed problem was proven to also be the optimal solution of Problem 2; however, this does not hold for thrust pointing constraints, even when $\theta \in [0, \pi/2)$. The theoretical contribution of this paper is the extension of the lossless convexification for Problem 2 to holds for thrust pointing constraints. Additionally, planetary rotation is included, which was not a part of Ref. [1].

The enhanced relaxed problem uses a slack variable $\Gamma(t)$ to relax all of the control constraints, which become

- Convex upper bound on thrust, $\|\mathbf{T}_c(t)\| \leq \Gamma(t)$.
- Convex thrust pointing constraint, $\hat{\mathbf{n}}^T \mathbf{T}_c(t) \geq \Gamma(t) \cos \theta$.
- Convex bounds on scalar Γ , $\rho_1 \leq \Gamma(t) \leq \rho_2$.

The relaxed pointing constraint forms a half-space of valid thrust values in \mathbf{T}_c - Γ space. The valid thrust values are in the direction of the outward facing normal to the half space:

$$\text{half-space normal} \triangleq \begin{pmatrix} \hat{\mathbf{n}} \\ -\cos \theta \end{pmatrix}, \quad (13)$$

which comes from the convex pointing-constraint inequality above. Figure 3 illustrates the half-space constraint for several pointing angles ($\theta = \{180^\circ, 90^\circ, 0^\circ\}$) and a planar (i.e., two-dimensional) thrust representation with pointing vector $\hat{\mathbf{n}}$ along the $\mathbf{T}_{c(1)}$ axis. The half-space orientation is significant as its intersection with the convex thrust-bound set provides the set of valid thrust profiles for the enhanced PDG algorithm. Reference [1] shows the convexified thrust bounds form a sliced 45° cone (Figure 4, left). Since the intersection of convex sets is also convex, the intersection of the relaxed thrust bounds and the relaxed pointing-constraint half-space forms a convex set. Figure 4 (right) shows intersection for a pointing-constraint half-space with $\theta > 90^\circ$.

Since the relaxed thrust bounds form a 45° cut cone, a pointing constraint of $\theta = 180^\circ$ (effectively no pointing constraint) will intersect the cone only on the line at the bottom 45° edge. Thus, the entire cut cone contains valid thrust values for the relaxed problem. Recall, the pointing

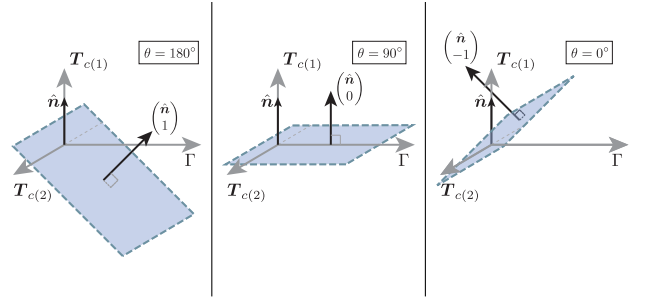


Fig. 3. The relaxed pointing constraint is convex. The set is a half-space in the direction on the normal vector to the planes shown for $\theta = 180^\circ$ (left), $\theta = 90^\circ$ (center), and $\theta = 0^\circ$ (right). Planar thrust is used here.

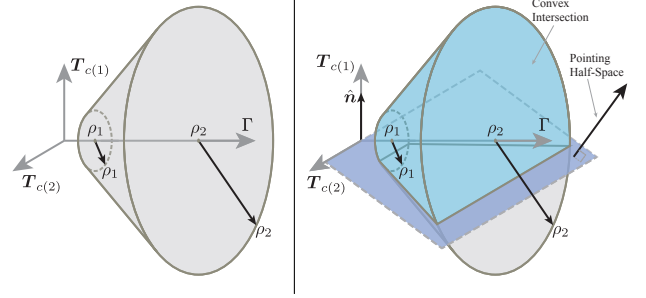


Fig. 4. Planar representation of thrust-bound relaxation (left) and its intersection with relaxed pointing-constraint half-space (right).

half-space is above the plane oriented at -45° to the Γ axis (Figure 3, left). In contrast, when $\theta = 0^\circ$ the pointing-constraint half-space is above the plane oriented at $+45^\circ$ to the Γ axis and intersects the relaxed thrust-bound cone on the upper 45° edge. Only this line has valid thrust values, which only apply to the extremely unlikely scenario of a vertical-only thrust for a descent directly above the target.

The relaxed thrust pointing constraints enhance the original relaxed PDG problem, which is given by

Problem 3: Relaxed minimum-fuel guidance problem

$$\min_{t_f, \mathbf{T}_c(\cdot), \Gamma(\cdot)} \int_0^{t_f} \Gamma(t) dt \quad (14)$$

subject to the following: for all $t \in [0, t_f]$,

$$\dot{\mathbf{x}}(t) = A(\hat{\omega})\mathbf{x}(t) + B \left(\mathbf{g} + \frac{\mathbf{T}_c(t)}{m(t)} \right), \quad (15)$$

$$\dot{m}(t) = -\alpha\Gamma(t), \quad (16)$$

$$\|\mathbf{T}_c(t)\| \leq \Gamma(t), \quad 0 < \rho_1 \leq \Gamma(t) \leq \rho_2, \quad (17)$$

$$\hat{\mathbf{n}}^T \mathbf{T}_c(t) \geq \Gamma(t) \cos \theta, \quad (18)$$

$$m(0) = m_0, \quad m(t_f) \geq m_0 - m_f > 0,$$

$$\mathbf{r}(0) = \mathbf{r}_0, \quad \dot{\mathbf{r}}(0) = \dot{\mathbf{r}}_0, \quad \mathbf{e}_1^T \mathbf{r}(t_f) = 0, \quad \dot{\mathbf{r}}(t_f) = \mathbf{0}$$

$$\mathbf{x}(t) \in \mathbf{X}, \quad \|\mathbf{E}\mathbf{r}(t_f) - \mathbf{q}\| \leq \|\mathbf{d}_{P1}^* - \mathbf{q}\|$$

where

$$\hat{\omega} := \begin{cases} \omega & \text{if } S(\omega)\hat{\mathbf{n}} \neq \mathbf{0}, \mathbf{N}^T S(\omega)^2 \hat{\mathbf{n}} \neq \mathbf{0} \\ \omega + \epsilon \hat{\mathbf{n}}^\perp & \text{if } S(\omega)\hat{\mathbf{n}} = \mathbf{0} \\ \omega + \epsilon \hat{\mathbf{n}} & \text{if } S(\omega)\hat{\mathbf{n}} \neq \mathbf{0}, \mathbf{N}^T S(\omega)^2 \hat{\mathbf{n}} = \mathbf{0} \end{cases} \quad (19)$$

with $\hat{\mathbf{n}}^\perp$ a unit vector such that $\hat{\mathbf{n}}^T \hat{\mathbf{n}}^\perp = 0$, $\mathbf{N} \in \mathbb{R}^{3 \times 2}$ has columns spanning the null space of $\hat{\mathbf{n}}^T$, and $\epsilon > 0$ is a small real number.

Note that the non-convex thrust constraints in (7) for Problems 2 and 1 have been replaced with convex constraints (16) and (17) in Problem 3. Also we modified the dynamics slightly, $\epsilon > 0$ can be chosen arbitrarily close to zero, when $S(\omega)\hat{n} = \mathbf{0}$. This is done purely for theoretical reasons that will enable us to prove Theorem 1 below. In practice we have not seen any case where this modification was needed. In Ref. [1] we showed that constraint relaxation (16) on the thrust bound allows the discrete-time form of Problem 3 to be posed as a convex optimization problem; the same holds true with the addition of the convex thrust-pointing constraint (17). Additionally note that the relaxation of the thrust-pointing constraint can also be applied to the precision-landing version of the convex algorithm in [2].

Definition 1: \mathcal{F}_e denotes the set of feasible solutions of Problem 1 and \mathcal{F}_f for Problem 2, that is, $\{t_f, \mathbf{T}_c, \mathbf{x}, m\} \in \mathcal{F}_e$ if it satisfies all the state (9), control (7), and fuel (8) constraints, dynamics (1), and boundary constraints (10) of the problem, and similarly for \mathcal{F}_f . $\mathcal{F}_e^* \subseteq \mathcal{F}_e$ and $\mathcal{F}_f^* \subseteq \mathcal{F}_f$ are the corresponding set of optimal solutions. \mathcal{F}_{rf} denotes the set of feasible solutions $\{t_f, \mathbf{T}_c, \Gamma, \mathbf{x}, m\}$ for Problem 3, with $\mathcal{F}_{rf}^* \subseteq \mathcal{F}_f$ being the set of optimal solutions.

Now, the following theorem gives a generalization of the earlier results in [1], [2] to also handle thrust pointing constraints.

Theorem 1: Consider Problem 3 with $\hat{\omega}$ as defined in (18). Let $\{t_f^*, \mathbf{T}_c^*, \Gamma^*, \mathbf{x}^*, m^*\} \in \mathcal{F}_{rf}^*$ such that the corresponding state trajectory $\mathbf{x}^*(t) \in \text{int}\mathbf{X} \forall t \in [0, t_f^*]$. Then, $\{t_f^*, \mathbf{T}_c^*, \mathbf{x}^*, m^*\} \in \mathcal{F}_f^*$.

The proof of Theorem 1 is contained in the Appendix. The above theorem states that the optimal solution of Problem 2 can be obtained by solving the relaxed Problem 3 for $\hat{\omega}$. Clearly for $\omega = \hat{\omega}$ we find the exact optimal solution to the problem of interest. When $\hat{\omega} \neq \omega$, we find optimal solutions of a problem that can be made arbitrarily close to the problem of interest by simply choosing $\epsilon > 0$ close enough to zero.

III. PINPOINT LANDING SIMULATIONS WITH THRUST POINTING CONSTRAINTS

The incorporation of the pointing constraints into the PDG algorithm ensures that the translational guidance does not require the spacecraft attitude to be oriented outside of a desired pointing cone. The enforcement of additional guidance constraints usually results in a trade off in some aspect of performance. For instance, as the pointing constraints are tightened, the required fuel and flight time generally increase due to the restricted pointing capability. This result will be seen in the following comparison simulations, which make use of an example spacecraft with the following properties (at powered-descent ignition):

$$m_0 = 2000 \text{ kg}, \quad m_f = 300 \text{ kg}, \quad (19)$$

$$\rho_1 = 0.2 T_{\max}, \quad \rho_2 = 0.8 T_{\max}, \quad (20)$$

$$T_{\max} = 24000 \text{ N}, \quad \alpha = 5 \times 10^{-4} \text{ s/m}, \quad (21)$$

where T_{\max} is the maximum-capable translational thrust magnitude. Note, the thrust limits coincide with a minimum and maximum throttle of 20% and 80%, respectively.

The initial state of the spacecraft, expressed in a surface-fixed guidance frame, is

$$\mathbf{r}_0 = \begin{bmatrix} 2400 \\ 450 \\ -330 \end{bmatrix} \text{ m}, \quad \dot{\mathbf{r}}_0 = \begin{bmatrix} -10 \\ -40 \\ 10 \end{bmatrix} \text{ m/s}, \quad (22)$$

and the target landing site is at $\mathbf{q} = \mathbf{0}$ m, the origin of the guidance frame. The Mars parameters, also expressed in the guidance frame, are as follows:

$$\mathbf{g} = \begin{bmatrix} -3.71 \\ 0 \\ 0 \end{bmatrix} \text{ m/s}^2 \quad \text{and} \quad \boldsymbol{\omega} = \begin{bmatrix} 2.53 \times 10^{-5} \\ 0 \\ 6.62 \times 10^{-5} \end{bmatrix} \text{ rad/s}. \quad (23)$$

Note, since $S(\omega)\hat{n} \neq \mathbf{0}$, $\hat{\omega} = \omega$ in Problem 3.

Three simulations were run for varying pointing-constraint limits: i) unconstrained; ii) 90° constraint; iii) 45° constraint. The results of these simulations are overlaid in Figures 5–7. Figure 5 overlays the thrust pointing profiles for the duration of each guidance-profile flight time. As seen in the plot, the pointing angle is relative to local vertical, which aligns the pointing cone \hat{n} vector along the coordinate-frame X axis. The pointing profiles clearly indicate that the relaxed algorithm enforces the prescribed pointing constraints.

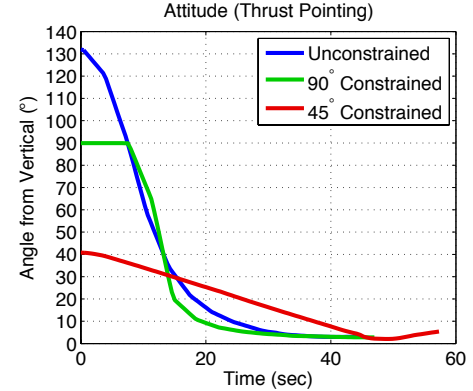


Fig. 5. Attitude constraints are enforced with the enhanced Powered-Descent Guidance algorithm

Figure 6 provides the throttle profiles that coincide with the pointing profiles of Figure 5. As seen in the throttle plot, all thrust bounds are obeyed during the simulations, which indicates that the constraint relaxations in Problem 3 on both thrust magnitude and pointing remains valid for the original pinpoint-landing problem (Problem 2). This figure provides some further insight on the trade off in performance that generally occurs as constraints are tightened. As the the pointing limit tightens, the required flight time and fuel increases, as summarized in Table I.

TABLE I
TIGHTENING POINTING CONSTRAINTS AFFECTS FUEL AND FLIGHT TIME

Attitude	Required Fuel (kg)	Flight Time (sec)
Unconstrained	200.1	44.63
90° Constraint	201.8	46.96
45° Constraint	222.3	57.29

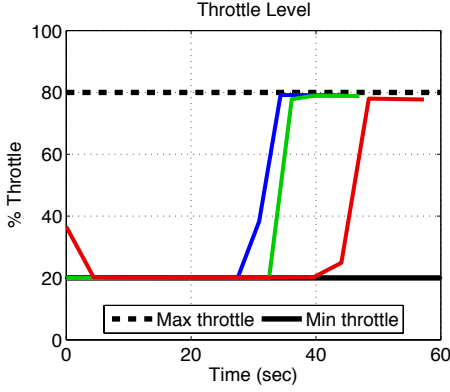


Fig. 6. Throttle constraints are obeyed for all attitude constraints

The impact of tighter pointing constraints is also visible in the ground track of the guidance profile along the Martian surface. Figure 7 overlays the surface trajectories coinciding with the three thrust profiles from the prior figures. The 45° constraint overshoots the target along the Y axis in order to satisfy the pointing constraint. Interestingly, the 90° constraint profile takes a more direct route to the target. This is a result of the optimization within Problem 3 that finds the profiles that minimize the fuel usage for pinpoint landing subject to the enforced constraints.

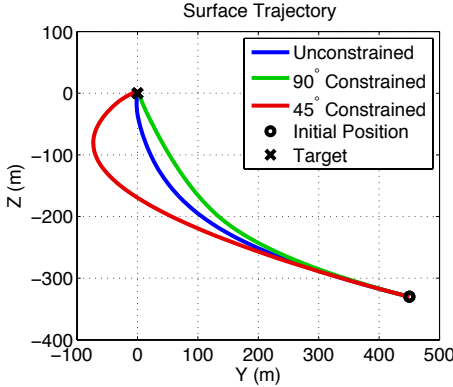


Fig. 7. Trajectories change with different attitude constraints

IV. CONCLUSIONS

A key development in numerically-efficient, convex Mars powered-descent guidance was presented within this paper. A theoretical extension of the relaxation that allows for convexification of minimum thrust bounds also provides for a lossless convexification of thrust pointing constraints, a significant contribution. The resultant, enhanced algorithm retains convexity and is valid for the original powered-descent guidance problem that has both upper and lower bounds on thrust as well as pointing constraints. Such pointing constraints can result from onboard sensor systems requiring specific fields of view to obtain terrain-relative state information, which is critical for enabling pinpoint and precision landing capability. In addition to the pointing constraints, the enhanced powered-descent guidance algorithm

accounts for planetary rotation in the dynamics and maintains the capability to enforce additional constraints on the state, including speed limits, glide-slope constraints, and surface constraints to avoid subsurface flight.

APPENDIX: PROOF OF THEOREM 1

The following two Lemmas are instrumental in the proof of Theorem 1. For brevity, they are stated without proof.

Lemma 1: Consider the following linear time invariant system

$$\dot{\boldsymbol{\lambda}}(t) = -A(\hat{\boldsymbol{\omega}})^T \boldsymbol{\lambda}(t), \quad \mathbf{y}(t) = B^T \boldsymbol{\lambda}(t), \quad (24)$$

where $\boldsymbol{\lambda}(t) \in \mathbb{R}^6$ and $\mathbf{y}(t) \in \mathbb{R}^3$, and $A(\hat{\boldsymbol{\omega}})$ and B are given by (2). Then the following conditions hold true; for any finite interval $[0, t_f]$:

- (i) \mathbf{y} is an analytic function, and $\mathbf{y}(t) = \mathbf{0}$ on either $[0, t_f]$ or at countable number of instances.
- (ii) There is a countable number of instances in $[0, t_f]$ such that $\mathbf{y}(t) = \alpha(t)\hat{\mathbf{n}}$ for some $\alpha(t) > 0$.

Lemma 2: An optimal solution of the following optimization problem is also an extreme point of the feasible set of solutions $\mathbf{U}(\Gamma)$:

$$\max_{\mathbf{T}_c} \mathbf{y}^T \mathbf{T}_c \quad \text{subject to} \quad \mathbf{T}_c \in \mathbf{U}(\Gamma)$$

where $\mathbf{U}(\Gamma) := \{\mathbf{T}_c : \|\mathbf{T}_c\| \leq \Gamma, \hat{\mathbf{n}}^T \mathbf{T}_c \geq \cos \theta\}$, and $\mathbf{y} \neq \mathbf{0}$ and $\mathbf{y} \neq -\alpha\hat{\mathbf{n}}$ for any $\alpha > 0$. Consequently an optimal solution \mathbf{T}_c^* satisfies that $\|\mathbf{T}_c^*\| = \Gamma$.

Proof: [for Theorem 1] Let $\tilde{\mathbf{q}} := E\mathbf{r}^*(t_f^*)$. Then, we can consider $\{t_f^*, \mathbf{T}_c^*, \Gamma^*, \mathbf{x}^*, m^*\}$ as an optimal solution of Problem 3 where the constraint $\|E\mathbf{r}(t_f) - \mathbf{q}\| \leq \|d_{P1}^* - \mathbf{q}\|$ is replaced by $E\mathbf{r}(t_f) = \tilde{\mathbf{q}}$. Without loss of any generality, this version of Problem 3 will be used in this proof.

Since $\mathbf{x}^*(t) \in \text{int}\mathbf{X}$ and $m(t) > m_0 - m_f$ for all $t \in [0, t_f]$, the Maximum Principle of optimal control (See Section V.3 of [14] or Chapter 1 of [15]), there exists a constant $\beta \leq 0$ and absolutely continuous function $\boldsymbol{\lambda} : \mathbb{R}_+ \rightarrow \mathbb{R}^6$ and $\eta : \mathbb{R}_+ \rightarrow \mathbb{R}$, the co-state vectors, such that the following conditions hold:

- (i) *Co-state conditions:* $\forall t \in [0, t_f]$,

$$(\beta, \boldsymbol{\lambda}(t), \eta(t)) \neq \mathbf{0} \quad (25)$$

$$\dot{\boldsymbol{\lambda}}(t) = -A(\hat{\boldsymbol{\omega}})^T \boldsymbol{\lambda}(t) \quad (26)$$

$$\dot{\eta}(t) = \frac{\boldsymbol{\lambda}(t)^T B \mathbf{T}_c(t)}{m(t)^2} \quad (27)$$

- (ii) *Pointwise Maximum Principle:*

$$H(\phi(t)) = M(\mathbf{x}^*(t), m^*(t), \boldsymbol{\lambda}(t), \eta(t)) \quad \text{a.e. } t \in [0, t_f^*] \quad (28)$$

where $\phi(t) = (t, \mathbf{x}^*(t), m^*(t), \mathbf{T}_c^*(t), \Gamma^*(t), \boldsymbol{\lambda}(t), \eta(t))$, H is the Hamiltonian defined by

$$H(\phi) := \beta\Gamma + \boldsymbol{\lambda}^T (A(\hat{\boldsymbol{\omega}})\mathbf{x} + B(\mathbf{g} + \mathbf{T}_c/m)) - \alpha\Gamma\eta \quad (29)$$

and, by letting $\mathbf{V} := \{(\mathbf{T}_c, \Gamma) \in \mathbb{R}^4 : \|\mathbf{T}_c\| \leq \Gamma, \rho_1 \leq \Gamma \leq \rho_2, \hat{\mathbf{n}}^T \mathbf{T}_c \geq \Gamma \cos \theta\}$,

$$M(\mathbf{x}^*, m^*, \boldsymbol{\lambda}, \eta) = \max_{(\mathbf{T}_c, \Gamma) \in \mathbf{V}} H(\phi). \quad (30)$$

(iii) *Transversality Conditions:*

$$\eta(t_f^*) = 0 \quad \text{and} \quad H(\phi(t_f^*)) = 0. \quad (31)$$

The necessary conditions of optimality (i) and (ii) directly follow from the statement of the Maximum Principle. But the transversality condition requires further explanation. Transversality condition implies that (See Section V.3 of [14]), for an optimal solution of the relaxed problem, the vector ψ , defined by

$$\psi := (H(\phi(0)), H(\phi(t_f^*)), -\lambda(0), -\eta(0), \lambda(t_f^*), \eta(t_f^*)),$$

must be orthogonal to the manifold defined by the set of feasible initial and final states described by $(0, t_f, \mathbf{x}_0, m_0, (0, \tilde{\mathbf{q}}, \mathbf{0}), m(t_f^*))$, which is given by

$$\text{span} \{e_2, e_{14}\}.$$

The above follows from the fact that t_f and $m(t_f)$ are the only free variables in the manifold of boundary conditions. This then implies that $e_2^T \psi = 0$ and $e_{14}^T \psi = 0$, that is, $H(\phi(t_f^*)) = 0$ and $\eta(t_f^*) = 0$.

Next we show that

$$\mathbf{y}(t) := B^T \boldsymbol{\lambda}(t) \neq \mathbf{0} \quad \text{a.e.} \quad [0, t_f^*]. \quad (32)$$

This will be done by contradiction. Suppose that the condition (32) does not hold. Since \mathbf{y} is an output of the system given by (26), $\mathbf{y}(t) = \mathbf{0}, \forall t \in [0, t_f^*]$, or $\mathbf{y}(t) = \mathbf{0}$ occurs at a countable number of points in $[0, t_f^*]$, which follows from the first conclusion of Lemma 1. Suppose $\mathbf{y}(t) = \mathbf{0} \forall t \in [0, t_f^*]$. Note that the pair $(A(\omega), B)$ is controllable, which follows from the fact that $[B \ A(\tilde{\omega})B]$ is an invertible matrix. Hence the pair $(B^T, -A(\tilde{\omega})^T)$ is observable. Consequently, $\mathbf{y}(t) = \mathbf{0} \forall t \in [0, t_f^*]$ implies that $\boldsymbol{\lambda}(t) = \mathbf{0} \forall t \in [0, t_f^*]$. Hence $\dot{\eta}(t) = 0 \forall t \in [0, t_f^*]$. Since $\eta(t_f^*) = 0$, this then implies that $\eta(t) = 0 \forall t \in [0, t_f^*]$. These imply $H(\phi(t)) = \beta \Gamma(t)$. Since $H(\phi(t_f^*)) = 0$ and $\Gamma(t) \geq \rho_1 > 0$, this suggests that $\beta = 0$. Therefore $(\beta, \boldsymbol{\lambda}(t), \eta(t)) = 0 \forall t \in [0, t_f^*]$, which is a contradiction with necessary Condition (i) above. Consequently there are countably many number of points in $[0, t_f^*]$ where $\mathbf{y}(t) = \mathbf{0}$. Since a countable set has measure zero, condition (32) holds.

Since any countable set has measure zero, the second conclusion of Lemma 1 implies that the, for any function α ,

$$\mathbf{y}(t) \neq -\alpha(t) \hat{\mathbf{n}} \quad \text{a.e.} \quad [0, t_f^*], \quad \alpha(t) > 0. \quad (33)$$

Since condition (32) holds, a.e. $[0, t_f^*]$ such that $\mathbf{y}(t) \neq \mathbf{0}$, and for a given $\Gamma^*(t)$ an optimal control thrust $\mathbf{T}_c^*(t)$ must satisfy

$$\mathbf{T}_c^*(t) = \arg \max_{(\mathbf{T}_c, \Gamma^*(t)) \in \mathbf{V}} \mathbf{y}(t)^T \mathbf{T}_c = \arg \max_{\mathbf{T}_c \in \mathbf{U}(\Gamma^*)} \mathbf{y}(t)^T \mathbf{T}_c, \quad (34)$$

where $\mathbf{U}(\Gamma) := \{\mathbf{T}_c \in \mathbb{R}^3 : \|\mathbf{T}_c\| \leq \Gamma, \hat{\mathbf{n}}^T \mathbf{T}_c \geq \Gamma \cos \theta\}$. Furthermore, since condition (33) holds, a.e. $[0, t_f^*]$ such that $\mathbf{y}(t) \neq \mathbf{0}$ and $\mathbf{y}(t) \neq -\alpha(t) \hat{\mathbf{n}}$ for some $\alpha(t) > 0$, the maximizing solution of (34) must be on the boundary point of $\mathbf{U}(\Gamma^*)$ that is also an extremal point of the set $\mathbf{U}(\Gamma^*)$, which follows from Lemma 2. This lemma also implies that

all the extremal points of the set $\mathbf{U}(\Gamma)$ satisfy $\|\mathbf{T}_c\| = \Gamma$, and hence we must have $\|\mathbf{T}_c^*(t)\| = \Gamma^*(t)$, that is,

$$\|\mathbf{T}_c^*(t)\| = \Gamma^*(t) \quad \text{a.e.} \quad [0, t_f^*], \quad (35)$$

which implies that an optimal solution of the relaxed problem (3) satisfies

$$0 < \rho_1 \leq \|\mathbf{T}_c^*(t)\| \leq \rho_2, \quad \text{a.e.} \quad [0, t_f^*], \\ \hat{\mathbf{n}}^T \mathbf{T}_c^*(t) \geq \|\mathbf{T}_c^*(t)\| \cos \theta$$

Consequently $(t_f^*, \mathbf{T}_c^*, \mathbf{x}^*, m^*) \in \mathcal{F}_f$. Since for any $(t_f, \mathbf{T}_c, \mathbf{x}, m) \in \mathcal{F}_f$, $(t_f, \mathbf{T}_c, \|\mathbf{T}_c\|, \mathbf{x}, m) \in \mathcal{F}_{rf}$, an optimal solution of Problem 3 has an optimal cost which is not greater than the optimal cost of Problem 2. This implies that $(t_f^*, \mathbf{T}_c^*, \mathbf{x}^*, m^*) \in \mathcal{F}_f^*$, which completes the proof. \blacksquare

ACKNOWLEDGEMENTS

We gratefully acknowledge Aron Wolf, Mark Ivanov, and Jordi Casoliva of the Jet Propulsion Laboratory for their valuable comments and suggestions. This research was performed at the Jet Propulsion Laboratory, California Institute of Technology, under a contract with the National Aeronautics and Space Administration.

REFERENCES

- [1] B. Açıkmeşe and S. R. Ploen, "Convex programming approach to powered descent guidance for mars landing," *AIAA Journal of Guidance, Control and Dynamics*, vol. 30, no. 5, pp. 1353–1366, 2007.
- [2] L. Blackmore, B. Açıkmeşe, and D. P. Scharf, "Minimum landing error powered descent guidance for mars landing using convex optimization," *AIAA Journal of Guidance, Control and Dynamics*, vol. 33, no. 4, 2010.
- [3] J. S. Meditch, "On the problem of optimal thrust programming for a lunar soft landing," *IEEE Transactions on Automatic Control*, vol. AC-9, no. 4, pp. 477–484, 1964.
- [4] A. Miele, *The Calculus of Variations in Applied Aerodynamics and Flight Mechanics in Optimization Techniques (G. Leitmann, ed.)*. Academic Press, New York, 1962.
- [5] A. R. Klumpp, "Apollo lunar descent guidance," *Automatica*, vol. 10, pp. 133–146, 1974.
- [6] U. Topcu, J. Casoliva, and K. Mease, "Minimum-fuel powered descent for mars pinpoint landing," *AIAA Journal of Spacecraft and Rockets*, vol. 44, no. 2, pp. 324–331, 2007.
- [7] R. Sostaric and J. Rea, "Powered descent guidance methods for the moon and mars," *AIAA Guidance, Navigation, and Control Conference, San Francisco, CA*, 2005.
- [8] F. Najson and K. Mease, "Computationally inexpensive guidance algorithm for fuel-efficient terminal descent," *AIAA Journal of Guidance, Control and Dynamics*, vol. 29, no. 4, pp. 955–964, 2006.
- [9] B. Steinfeldt, M. Grant, D. Matz, and R. Braun, "Guidance, navigation, and control technology system trades for mars pinpoint landing," in *AIAA Guidance, Navigation and Control Conference*, 2008.
- [10] C. D'Souza, "An optimal guidance law for planetary landing," in *AIAA Guidance, Navigation and Control Conference*, 1997.
- [11] S. Ploen, B. Acikmese, and A. Wolf, "A comparison of powered descent guidance laws for mars pinpoint landing," *AIAA Guidance, Navigation, and Control Conference, Keystone, CO*, 2006.
- [12] Y. Nesterov and A. Nemirovsky, *Interior-point Polynomial Methods in Convex Programming*. SIAM, 1994.
- [13] S. Boyd and L. Vandenberghe, *Convex Optimization*. Cambridge University Press, 2004.
- [14] L. D. Berkovitz, *Optimal Control Theory*. Springer-Verlag, 1975.
- [15] L. S. Pontryagin, V. G. Boltyanskii, R. V. Gamkrelidze, and E. F. Mishchenko, *The Mathematical Theory of Optimal Processes*. Pergamon Press, 1964.